

On the influence of multiple polarization changes on the cumulative deformations in sand under drained high-cyclic loading

T. Wichtmannⁱ⁾; Th. Triantafyllidisⁱⁱ⁾

Abstract: The effect of multiple changes of the polarization (i.e. direction) of a drained cyclic loading has been studied in about 50 triaxial tests with a simultaneous harmonic oscillation of the axial and the lateral stresses. A fine sand has been tested at various initial densities. Starting from the same average stress in all tests, six different polarizations of the cycles have been applied by choosing different amplitudes and phase shifts between the axial and the lateral stress component. In each test at least 10,000 cycles have been applied. The polarization has been changed every 1000, 2500 or 5000 cycles. The sequence of the polarizations has been varied from test to test. Several reference tests without polarization changes have been also performed. The test results reveal, that the first change of the polarization usually leads to a temporary increase of the rate of strain accumulation. This increase depends on the angle between the subsequent polarizations, while the correlation with density or the number of cycles applied prior to the polarization change is poor. All further polarization changes have only a minor effect on the rate of strain accumulation. Consequently, the final residual strain after 10,000 cycles is only moderately increased by the multiple polarization changes. The consequences of these experimental results for a high-cycle accumulation model describing the cumulative deformations in sand under a high-cyclic loading are briefly addressed.

Keywords: high-cyclic loading; multiple polarization changes; drained cyclic triaxial tests

1 Introduction

A high-cyclic loading is characterized by a large number of cycles ($N \geq 10^3$) and relative small strain amplitudes ($\varepsilon^{\text{ampl}} \leq 10^{-3}$). It may be caused by traffic (high-speed trains, magnetic levitation trains), industrial sources (crane rails, machine foundations), wind and waves (on-shore and off-shore wind power plants, coastal structures), repeated filling and emptying processes (locks, tanks and silos), construction processes (e.g. vibration of sheet piles) or mechanical compaction (e.g. vibratory compaction). Permanent deformations accumulated in the subsoil due to the high-cyclic loading may endanger the serviceability of foundations. Consequently, these long-term deformations have to be accurately predicted in the design stage. The high-cycle accumulation (HCA) model of Niemunis et al. [11] may be used for that purpose.

In case of wind and waves, the high-cyclic loading frequently changes its direction (also termed polarization). The effect of multiple polarization changes on the cumulative deformations has rarely been studied in element tests so far. Almost all experimental investigations of a high-cyclic loading documented in the literature so far, involving either element, model or field tests, have been performed with a constant direction of the cycles (e.g. [2, 4, 6–8, 12, 15–17, 26]). The first study giving hints that changes of the polarization of the cycles may accelerate stress relaxation under undrained conditions and strain accumulation in the drained case was that of Yamada & Ishihara [25]. Their true triaxial tests only comprised four cy-

cles of loading, however, i.e. they did not test a high-cyclic loading. In contrast to [25], Tokue [18] did not find a significant alteration of the compaction rate when the polarization was changed by 90° in the middle of a cyclic simple shear test.

Some multi-dimensional simple shear tests performed by the authors [19, 22] revealed that a change of the direction of the cycles by 90° leads to a temporary increase of the rate of strain accumulation (Figure 1). However, all tests in [19, 22] were restricted to a single change of the polarization by 90° . Based on these test results the function f_π of the HCA model (see equations in Appendix) describing the effect of polarization changes has been calibrated. Le [5] recently performed a parametric study with polarization changes in another simple shear test apparatus. In that study the angle between subsequent polarizations, the number of cycles prior to the polarization change, the density and the amplitudes prior and after the polarization change have been varied. Based on his test results Le proposed a modification of the original formulation for f_π . However, the tests of Le [5] were again restricted to a single change of the polarization.

Therefore, in order to investigate the effect of multiple polarization changes, the test series presented in this paper has been conducted. Considering the inhomogeneous fields of strain and stress usually encountered in simple shear tests [1], the new experimental study has been performed in the triaxial apparatus. The different polarizations have been achieved by a simultaneous harmonic oscillation of the axial and the lateral stress.

Model tests on pile foundations with changes of the direction of horizontal cyclic loading are documented e.g. in [3, 13, 14]. They are further addressed later in this paper.

ⁱ⁾Professor for Geotechnical Engineering, Bauhaus-Universität Weimar, Germany (corresponding author). Email: torsten.wichtmann@uni-weimar.de

ⁱⁱ⁾Professor and Director of the Institute of Soil Mechanics and Rock Mechanics, Karlsruhe Institute of Technology, Germany

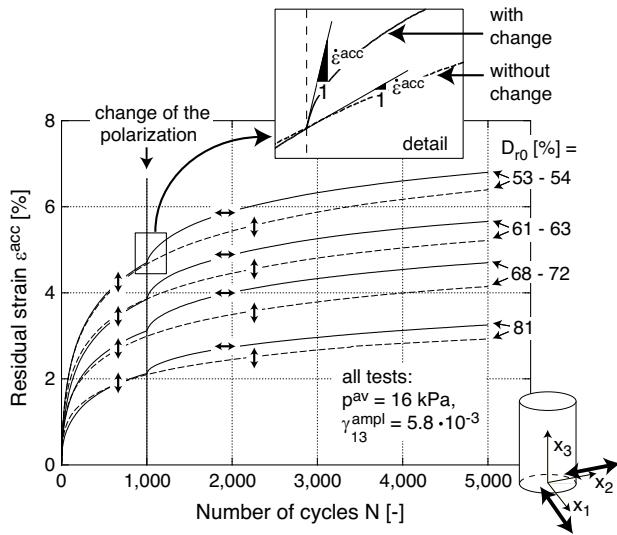


Fig. 1: Temporary increase of the strain accumulation rate due to a change of the shearing direction by 90° after 1000 cycles, measured in simple shear tests [22]

2 Description of tests

2.1 Test material

The test material is a fine sand obtained from the company "Gebrüder Willersinn GmbH & Co. KG" in Ludwigshafen, Germany. The grain size distribution curve is given in Figure 2. The mean grain size is $d_{50} = 0.14$ mm and the uniformity coefficient is $C_u = d_{60}/d_{10} = 1.5$. The minimum and maximum dry densities were determined according to German standard code DIN 18126 as $\rho_{d,min} = 1.290$ g/cm³ and $\rho_{d,max} = 1.580$ g/cm³, corresponding to void ratios $e_{min} = 0.677$ and $e_{max} = 1.054$. The grains have a sub-angular shape and the density $\rho_s = 2.65$ g/cm³.

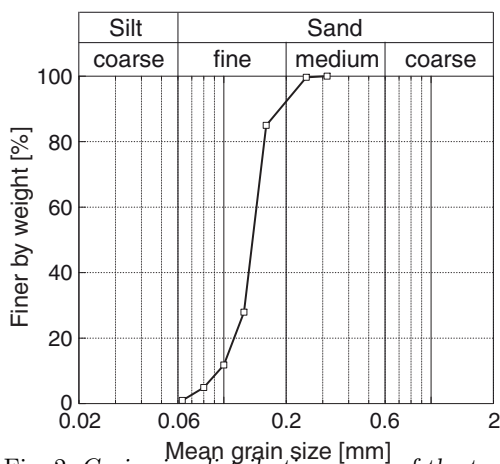


Fig. 2: Grain size distribution curve of the tested fine sand

2.2 Test device

A scheme of the cyclic triaxial device used for the present study is given in Figure 3. This triaxial device has been designed and manufactured at the institute of the authors with the aim to enable tests with very large numbers of cycles. The specimen is encompassed in a pressure cell being capable for pressures up to 1000 kPa. A pneumatic loading

system is used to apply the axial loading. The pneumatic cylinder is located at the bottom of the test device, so that the axial loading is applied in the upwards direction. This arrangement has the advantage that it enables a specimen preparation inside the test device, i.e. directly on the load piston (see the photos in Figure 4). The cell is completely filled with water. The cell pressure is applied pneumatically via an air-water interface, where air and water are separated by a membrane. Two electronically controlled mechanical valves are used to regulate the pressures in the pneumatic cylinder (axial loading) or the cell pressure (lateral loading), respectively.

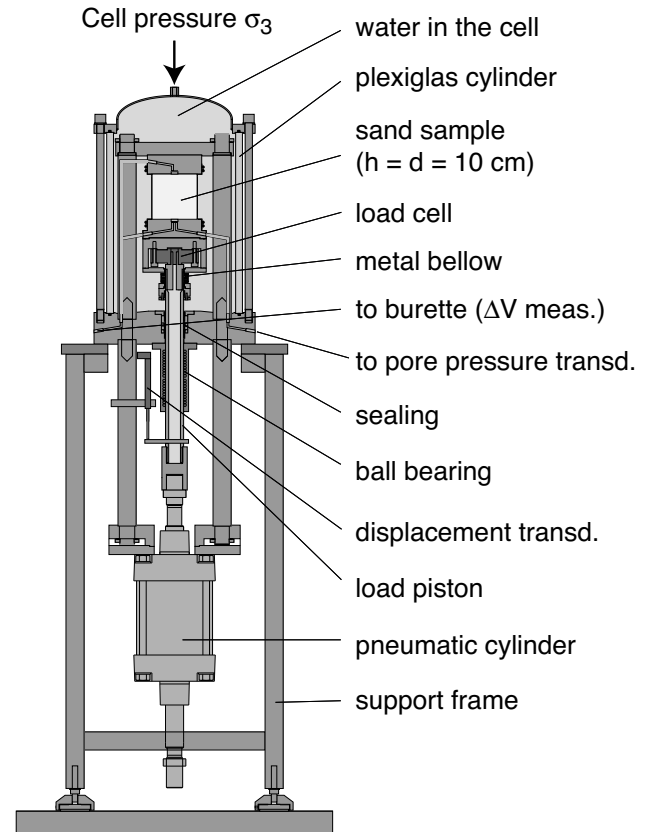


Fig. 3: Scheme of the cyclic triaxial device used for this study

The load is measured inside the pressure cell at a load cell located below the bottom end plate. The axial deformations are obtained from a displacement transducer attached to the load piston (Figure 3). The system compliance was determined in preliminary tests on a steel dummy and subtracted from the measured values. Volume changes were measured via the squeezed out pore water using a burette system and a differential pressure transducer (not shown in Figure 3). Two pressure transducers were used for monitoring cell pressure and back pressure. All signals were continuously recorded with a data acquisition system (100 records per cycle).

Specimens with a diameter of 100 mm and a height of 100 mm (height-to-diameter ratio $h/d = 1$) were used in the present test series. They are a standard at the IBF in Karlsruhe for triaxial testing in connection with constitutive modeling because they are assumed to deform more homogeneous than specimens with $h/d = 2$. In cyclic tests, due to the rather small deformations, specimens with h/d

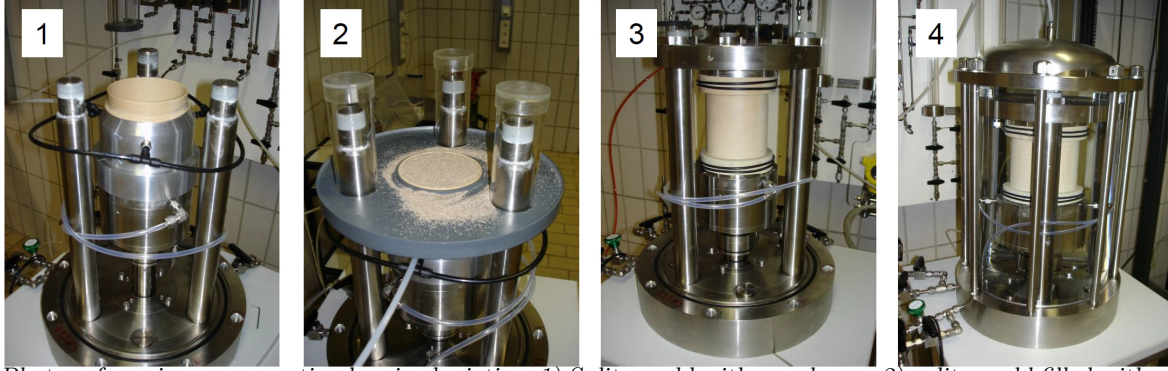


Fig. 4: Photos of specimen preparation by air pluviation: 1) Split mould with membrane, 2) split mould filled with sand, 3) specimen under vacuum after removal of split mould, 4) after mounting and filling of the cell

= 1 and 2 deliver almost identical results [20]. In order to eliminate end friction effects, smeared end plates composed of a layer of grease and an overlying rubber disk were applied. The bottom and the top end plates are both equipped with a central porous stone of 15 mm diameter connected with the drainage system.

All specimens were prepared by air pluviation out of a funnel. Some stages of the specimen preparation procedure are shown in Figure 4. Different outlet diameters of the funnel were applied to achieve different initial densities. After preparation the specimens were saturated with de-aired water. A back pressure of 500 kPa was used in all tests. Skempton's B value was larger than 0.99 for all specimens tested in the present study.

2.3 Tested stress and strain paths

After the B value test the specimens were loaded to the average effective stress with the axial component $\sigma_1^{\text{av}} = 266.67$ kPa and a lateral component $\sigma_3^{\text{av}} = 166.67$ kPa, resulting in average values of the effective mean pressure $p^{\text{av}} = (\sigma_1^{\text{av}} + 2\sigma_3^{\text{av}})/3 = 200$ kPa and the deviatoric stress $q^{\text{av}} = \sigma_1^{\text{av}} - \sigma_3^{\text{av}} = 100$ kPa. The average stress ratio thus is $\eta^{\text{av}} = q^{\text{av}}/p^{\text{av}} = 0.5$. The stress ratio has been chosen somewhat lower than the value $\eta^{\text{av}} = 0.75$ frequently applied in previous studies [19, 21, 23]. The intention of the choice of $\eta^{\text{av}} = 0.5$ was to increase the distance of the average stress to the critical state line (CSL) in the p - q diagram (stress ratio of CSL $\eta = M_c(\varphi_c) \approx 1.3$) and consequently minimize the effect of the polarization, because stress cycles with a maximum stress lying in the vicinity of the CSL could cause larger cumulative rates. After a resting period of one hour at the average stress the cyclic loading was started, i.e. the average components σ_1^{av} and σ_3^{av} of the axial and lateral stress were superposed by a sinusoidal cyclic portion with the amplitudes σ_1^{ampl} and σ_3^{ampl} (Figure 5a), i.e.

$$\sigma_1' = \sigma_1^{\text{av}} + \sigma_1^{\text{ampl}} \sin\left(\frac{2\pi}{T}t + \theta_1\right) \quad (1)$$

$$\sigma_3' = \sigma_3^{\text{av}} + \sigma_3^{\text{ampl}} \sin\left(\frac{2\pi}{T}t + \theta_3\right) \quad (2)$$

with time t , period T of the cycles and phase shifts θ_1 and θ_3 . The respective functions in terms of p and q , with

$p = (\sigma_1' + 2\sigma_3')/3$ and $q = \sigma_1' - \sigma_3'$, read

$$p = p^{\text{av}} + p^{\text{ampl}} \sin\left(\frac{2\pi}{T}t + \theta_p\right) \quad (3)$$

$$q = q^{\text{av}} + q^{\text{ampl}} \sin\left(\frac{2\pi}{T}t + \theta_q\right) \quad (4)$$

with phase shifts θ_p and θ_q . All cycles were applied with a loading frequency of $f = 0.01$ Hz, i.e. a period of $T = 100$ s.

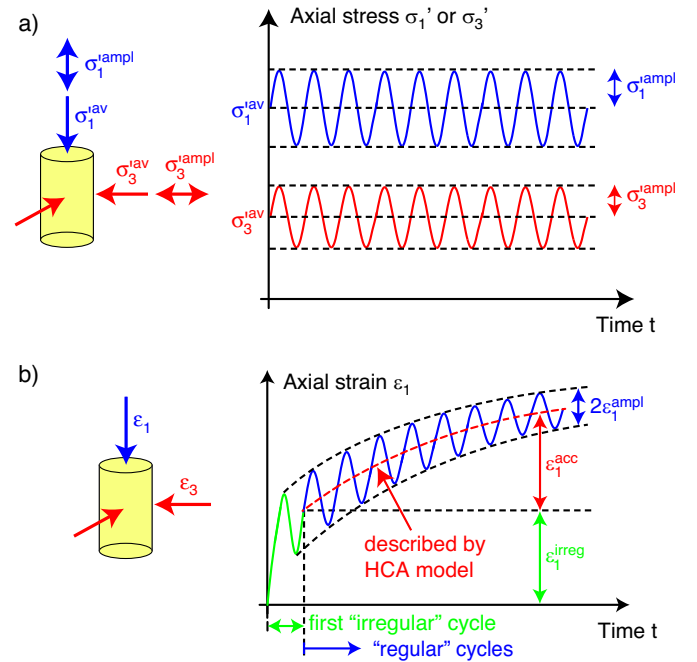


Fig. 5: Development of a) axial effective stress σ_1' and lateral effective stress σ_3' and b) axial strain ε_1 with time during the cyclic loading

Six different polarizations have been tested. The chosen stress amplitudes and phase shifts are summarized in Table 1. The stress paths for the different polarizations are shown in the p - q plane in Figure 6a while a presentation in the P - Q diagram is provided in Figure 6b. The isometric variables $P = \sqrt{3}p$ and $Q = \sqrt{3}/2q$ [10] are advantageous in connection with studies on the influence of the polarization because the lengths of the stress paths and the angles

between two polarizations are preserved when transferred from a principal stress coordinate system to the P - Q plane. In contrast, they are not preserved in case of the conventional p - q diagram. The time course of P and Q during the cycles is analogous to that of p and q described by Eqs. (3) and (4), with amplitudes P^{ampl} and Q^{ampl} and phase shifts $\theta_P = \theta_p$ and $\theta_Q = \theta_q$. In the present test series, two neighbored polarizations differed by an angle $\Delta\alpha_{PQ} = 30^\circ$ in the P - Q plane. Polarizations 1 and 4 were parallel to the P - or Q -axis, respectively, i.e. they represent purely isotropic or purely deviatoric stress cycles.

The development of strain with time during the cycles is shown schematically for the axial component ε_1 in Figure 5b. The first quarter of the first cycle represents a virgin loading of the specimen which usually causes larger residual deformations than the subsequent cycles. Therefore, it is distinguished between the first "irregular" and the following "regular" cycles. The strain during the regular cycles can be divided in a residual (accumulated, plastic) portion $\varepsilon_1^{\text{acc}}$ and an elastic portion (strain amplitude) $\varepsilon_1^{\text{ampl}}$.

Corresponding to the isometric stress invariants P and Q , the isometric strain components $\varepsilon_P = 1/\sqrt{3}\varepsilon_v$ and $\varepsilon_Q = \sqrt{3}/2\varepsilon_q$ are introduced, with volumetric strain $\varepsilon_v = \varepsilon_1 + 2\varepsilon_3$ and deviatoric strain $\varepsilon_q = 2/3(\varepsilon_1 - \varepsilon_3)$. The intended strain paths during the cycles are shown schematically in the ε_v - ε_q diagram in Figure 6c and in the isometric ε_P - ε_Q plane in Figure 6d. The cycles were applied stress-controlled. Based on preliminary tests the stress amplitudes given in Table 1 have been chosen in order to achieve a strain amplitude $\varepsilon^{\text{ampl}} = \sqrt{(\varepsilon_P^{\text{ampl}})^2 + (\varepsilon_Q^{\text{ampl}})^2} \approx 4 \cdot 10^{-4}$ for all six polarizations at a medium density $D_{r0} = (e_{\text{max}} - e_0)/(e_{\text{max}} - e_{\text{min}}) \cdot 100 \approx 60\%$ (see scheme in Figure 6d or test data in Figure 8d). This strain amplitude is representative for a high-cyclic loading and lies within the ranges tested in previous studies of the authors [19, 22].

Since the HCA model describes the strain accumulation rates during the regular cycles only (see the red dashed curve in Figure 5b), only the data from the regular cycles are discussed in this paper. In the following, $N = 1$ thus refers to the end of the first regular cycle (Figure 5b). With reference to the equations of the HCA model (see Appendix), in the interpretation of the test results it is distinguished between the *intensity* of accumulation, described by the total accumulated strain $\varepsilon^{\text{acc}} = \sqrt{(\varepsilon_1^{\text{acc}})^2 + 2(\varepsilon_3^{\text{acc}})^2}$ or its rate $\dot{\varepsilon}^{\text{acc}} = \partial\varepsilon^{\text{acc}}/\partial N$, and the *direction* of accumulation, expressed by the ratio of the volumetric ($\varepsilon_v^{\text{acc}}$) or deviatoric ($\varepsilon_q^{\text{acc}}$) accumulated strains.

2.4 Testing program

52 tests with initial relative densities (measured at p^{av} , q^{av} prior to the regular cycles) in the range $42\% \leq D_{r0} \leq 84\%$ have been performed, among them 41 with multiple polarization changes and 11 reference tests with a constant polarization throughout the test. The 20 different sequences applied in the tests with polarization changes are summarized in Table 2 and illustrated in Figure 7. In case of sequences Nos. 1 to 5 the polarization was changed every 1000 cycles. All six polarizations were involved in the first four sequences while only purely isotropic and purely deviatoric stress cycles (polarizations 1 and 4) were alternately applied in the tests with the fifth sequence. The polarization was altered every 2500 cycles in case of sequences Nos. 6 to

16, while 5000 cycles with a certain polarization were applied in case of sequences Nos. 17 to 20. For each sequence at least one test with a medium initial density has been performed ($53\% \leq D_{r0} \leq 69\%$, see last column in Table 2). For selected sequences a lower ($42\% \leq D_{r0} \leq 52\%$) and a higher ($77\% \leq D_{r0} \leq 84\%$) density were additionally tested. In few cases, in order to test reproducibility, two tests with loose or dense initial state were conducted. The reference tests were also performed with a wide range of initial densities ($42\% \leq D_{r0} \leq 77\%$). In these tests 11,000 cycles were applied along polarizations 1, 4 or 5. In all tests a total number of at least 10,000 cycles has been applied.

3 Analysis of the first 1,000 cycles: No influence of the polarization

The influence of the polarization itself can be examined based on the first 1000 cycles of each test, since the first polarization change was applied at $N \geq 1000$. In Figure 8a the curves of accumulated strain $\varepsilon^{\text{acc}}(N)$ measured in six tests with similar initial density but different polarizations are compared. No clear tendency regarding a possible influence of the polarization on the curves $\varepsilon^{\text{acc}}(N)$ can be found in that diagram. An inspection based on the data of all tests is undertaken in Figure 8b, where the residual strain ε^{acc} after 1000 cycles is shown as a function of the initial relative density. Despite some scatter this diagram confirms that for a given D_{r0} the residual strain is only marginally affected by the polarization. Also the direction of strain accumulation is independent of the polarization (Figure 8c), since the data of the accumulated deviatoric strain $\varepsilon_q^{\text{acc}}$ versus the accumulated volumetric strain $\varepsilon_v^{\text{acc}}$ for the different polarizations fall together on the same line. Based on the knowledge that the polarization itself does not significantly affect the cumulative deformations, next the influence of *changes* of the polarization can be studied.

4 Influence of polarization changes

Figures 9 and 10 present the curves of accumulated strain $\varepsilon^{\text{acc}}(N)$ during the complete tests. The diagrams in Figure 9 contain data for medium dense sand ($53\% \leq D_{r0} \leq 70\%$), while the data for either lower ($42\% \leq D_{r0} \leq 52\%$) or higher densities ($70\% \leq D_{r0} \leq 84\%$) are provided in Figure 10. In case of the medium dense specimens, the diagram in Figure 9a collects the data from the tests with polarization changes every 1000 cycles (sequences Nos. 1 - 5 in Figure 7), while those for the packages with 2500 and 5000 cycles are provided in Figure 9b-d (sequences Nos. 6 - 20). The diagrams in Figure 10 present the curves for more than one polarization change (sequences Nos. 1 - 16) on the left-hand side and those for only one change in the middle of the test (sequences Nos. 17 - 20) on the right-hand side. In Figures 9 and 10 the different polarizations are distinguished by choosing the same colours as used in Figures 6 and 7. For comparison purpose, the data from the reference tests without polarization changes (1D tests) performed on specimens with similar initial density have been added in each diagram of Figures 9 and 10. The differences between the curves $\varepsilon^{\text{acc}}(N)$ obtained in the individual tests being visible in Figures 9 and 10 are primarily due to the variations in initial densities. For all tested densities, a temporary increase of the rate of strain accumulation usually occurred due to the first change of the polarization only (see marked

Polarization	α_{PQ} [°]	α_{pq} [°]	σ_1^{ampl} [kPa]	θ_1 [-]	σ_3^{ampl} [kPa]	θ_3 [-]	p^{ampl} [kPa]	θ_p [-]	q^{ampl} [kPa]	θ_q [-]	P^{ampl} [kPa]	Q^{ampl} [kPa]
1	0	0.0	57.3	0	57.3	0	57.3	0	0.0	0	99.3	0.0
2	30	50.8	81.5	0	26.5	0	44.8	0	54.9	0	77.7	44.8
3	60	74.8	60.6	0	4.0	π	17.6	0	64.6	0	30.4	52.7
4	90	90.0	41.6	0	20.8	π	0.0	0	62.4	0	0.0	51.0
5	120	105.2	21.8	0	33.4	π	15.0	π	55.2	0	26.0	45.1
6	150	129.2	6.1	π	46.6	π	33.1	π	40.5	0	57.3	33.1

Table 1: Angles α_{PQ} and α_{pq} towards the horizontal in the P - Q or p - q plane, amplitudes and phase shifts of axial and lateral effective stress (σ_1^{ampl} , θ_1 , σ_3^{ampl} , θ_3), of mean effective stress and deviatoric stress (p^{ampl} , θ_p , q^{ampl} , θ_q) or of isometric stress variables (P^{ampl} , Q^{ampl} , with $\theta_P = \theta_p$ and $\theta_Q = \theta_q$) for the six tested polarizations

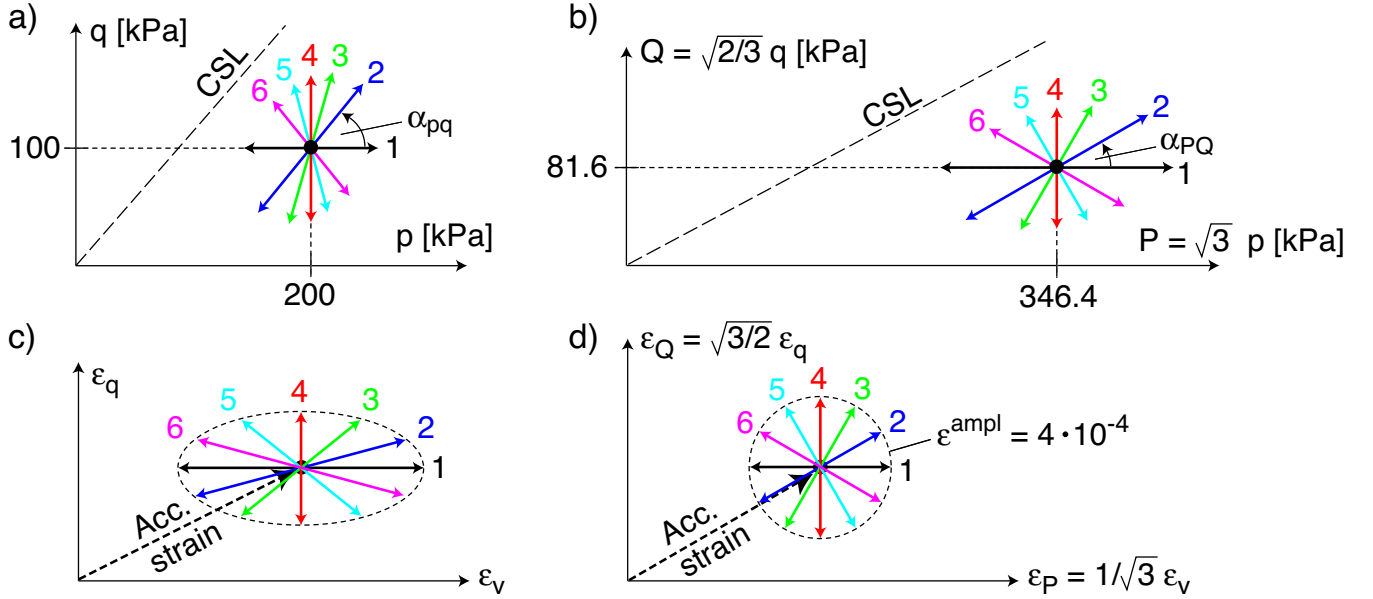


Fig. 6: Stress and strain paths in the tests with multiple polarization changes

No.	Sequence of polarizations	Number of cycles		Tested densities D_{r0} [%]
		per polar.	total	
1	1 → 2 → 3 → 4 → 5 → 6 → 5 → 4 → 3 → 2 → 1	1000	11,000	42 / 57 / 81
2	1 → 2 → 3 → 4 → 5 → 6 → 1 → 2 → 3 → 4 → 5 → 6			64
3	4 → 3 → 5 → 2 → 6 → 1 → 6 → 2 → 5 → 3 → 4			53
4	1 → 4 → 2 → 6 → 5 → 3 → 1 → 4 → 2 → 5 → 1			59
5	1 → 4 → 1 → 4 → 1 → 4 → 1 → 4 → 1 → 4 → 1			47 / 68 / 83
6	1 → 2 → 3 → 4	2500	10,000	58
7	4 → 3 → 2 → 1			61
8	2 → 3 → 4 → 5			45 / 61 / 77 / 79
9	3 → 4 → 5 → 6			63
10	6 → 5 → 4 → 3			56
11	2 → 5 → 3 → 6			61
12	5 → 2 → 6 → 3			62
13	1 → 3 → 5 → 1			49 / 61 / 79
14	3 → 1 → 5 → 3			59
15	1 → 4 → 1 → 4			49 / 64 / 84
16	4 → 1 → 4 → 1			69
17	1 → 4	5000	10,000	47 / 69 / 77
18	4 → 1			46 / 48 / 61 / 80
19	3 → 6			52 / 65 / 79 / 80
20	6 → 3			50 / 59 / 82

Table 2: Tested sequences of polarizations, numbers of cycles per package or whole test and initial relative densities D_{r0} of the specimens. The numbering of the six polarizations is illustrated in Figure 6.

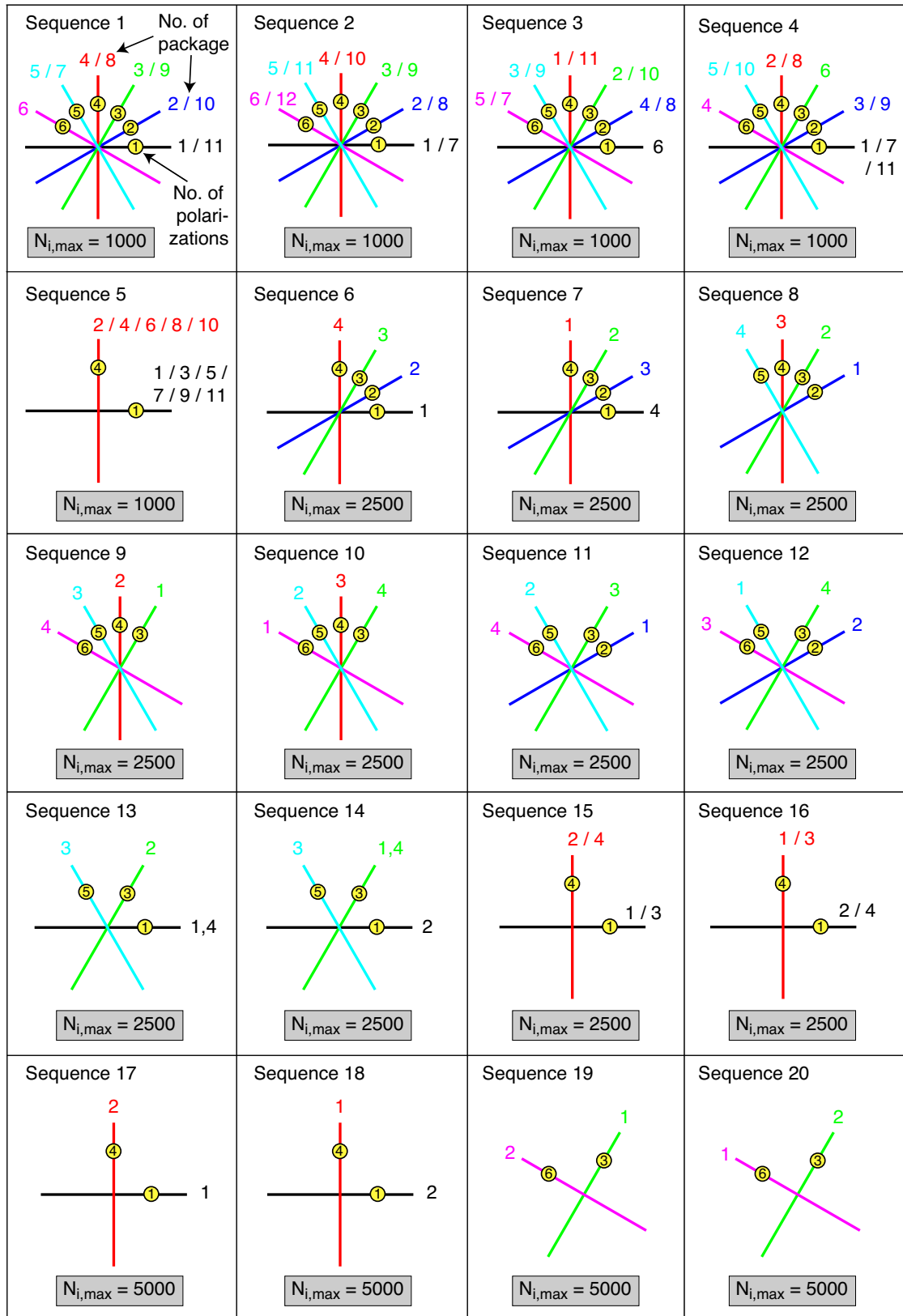


Fig. 7: Sequences of polarizations applied in the tests ($N_{i,max}$ = number of cycles in each package with a certain polarization)

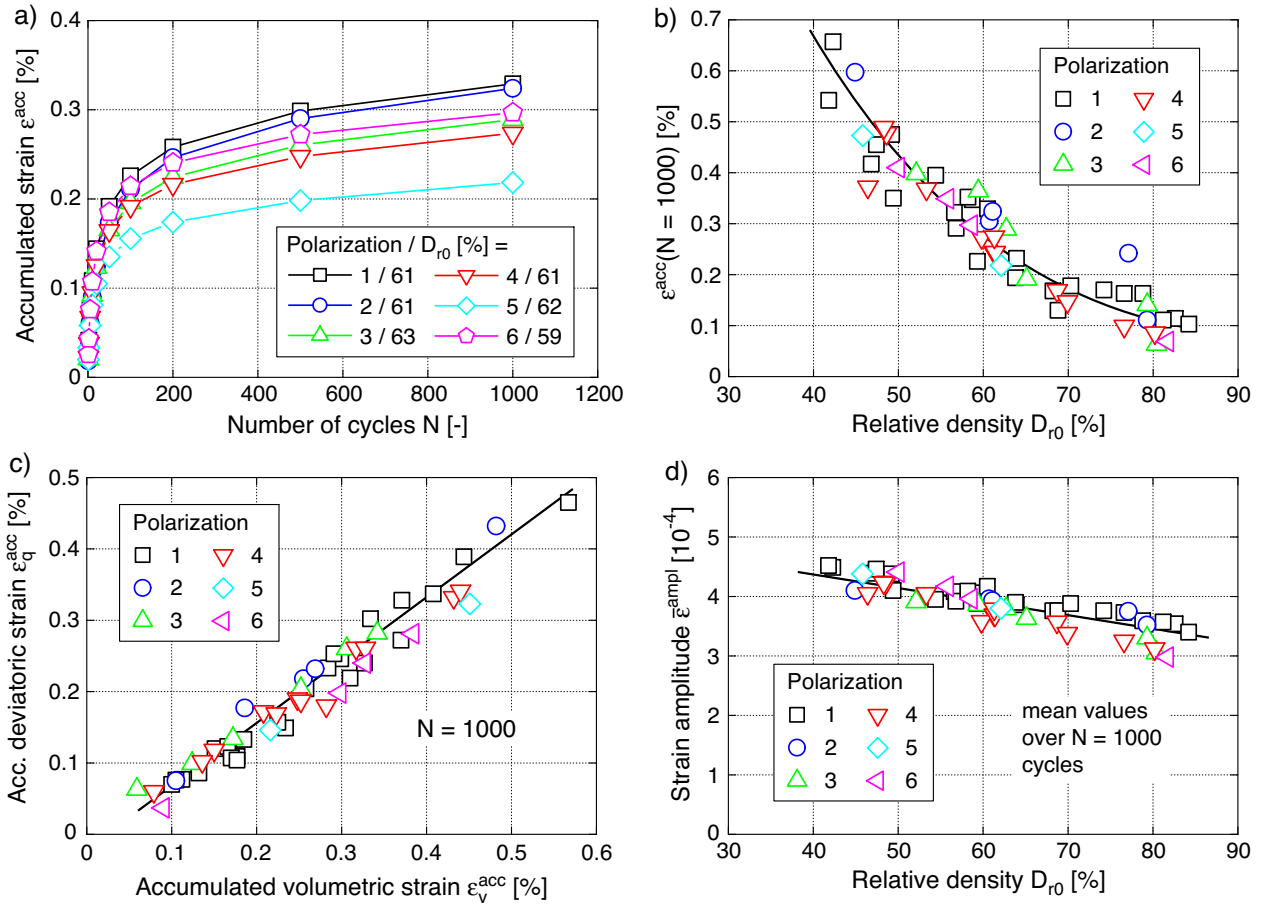


Fig. 8: Influence of the polarization on the cumulative and elastic strains during the first 1000 cycles: a) Strain accumulation curves $\epsilon^{acc}(N)$ measured in six tests with similar initial density but different polarizations, b) Accumulated strain ϵ^{acc} after 1000 cycles as a function of initial relative density D_{r0} , c) Accumulated deviatoric strain ϵ_q^{acc} as a function of accumulated volumetric strain ϵ_v^{acc} after 1000 cycles, d) Mean values of strain amplitude $\bar{\epsilon}^{ampl}$ during 1000 cycles in dependence of D_{r0}

rectangles in Figures 9 and 10). All subsequent alterations of the cyclic loading direction had only a moderate impact on the further course of the curves $\epsilon^{acc}(N)$.

The explanations of the experimental observations need to be sought in micromechanics. Some ideas on possible mechanisms are described in the following. They have to be confirmed by a quantitative analysis in future, which goes beyond the scope of the present study. A cyclic loading leads to subtle changes in the orientations of the grains or grain contact normals, usually rendering the sand fabric more stable to the subsequent cycles applied in the same direction, i.e. leading to an adaptation of the fabric to the actual cyclic loading. The consequence is a continuous reduction of the strain accumulation rate $\dot{\epsilon}^{acc}$ with increasing number of cycles, as evident from the nonlinear curves $\epsilon^{acc}(N)$ in Figures 8a, 9 and 10. In the HCA model this adaptation of the fabric is phenomenologically captured by the preloading variable g^A (see Appendix). If the direction of the cycles is altered, the grain skeleton starts to adapt to this new loading direction, showing larger strain accumulation rates directly after the polarization change, due to a larger potential for grain reorientations. After a certain number of cycles applied in the new direction, similar rates as before the polarization change are reached again, since a similar degree of adaptation of the fabric has been established in the new direction. The larger the angle between

the two subsequent polarizations involved in the first polarization change, the larger is the increase in potential for new grain reorientations. If the polarization of the cyclic loading returns to a direction already tracked during an earlier package of cycle (or to a similar polarization deviating by a relatively small angle $\Delta\alpha_{PQ}$ only), the adaptation of the fabric in that direction established during the earlier cyclic loading seems to be intact. As a consequence no further increase of the strain accumulation rate is observed in such cases. The memory of a sand regarding its cyclic preloading history may be erased by a monotonic loading as recently demonstrated by the experimental study presented in [24], but evidently not by multiple changes of the polarization.

The $\epsilon^{acc}(N)$ data in Figures 9 and 10 give hints that the temporary increase of the cumulative rate $\dot{\epsilon}^{acc}$ due to the first change of the polarization is more pronounced if the polarization is changed from a purely isotropic to a purely deviatoric direction than vice versa. A further inspection is undertaken in Figure 11 where the quotient of the rates of strain accumulation $\dot{\epsilon}^{acc} \approx \Delta\epsilon^{acc}/\Delta N$ before (evaluated from the last 500 cycles of the preceding bundle) and after (evaluated from the first 100 cycles of the subsequent bundle) the first polarization change is plotted in dependence of the angle $\Delta\alpha_{PQ}$ between both polarizations. For example, a change from polarization 1 (isotropic) to 4 (deviatoric)

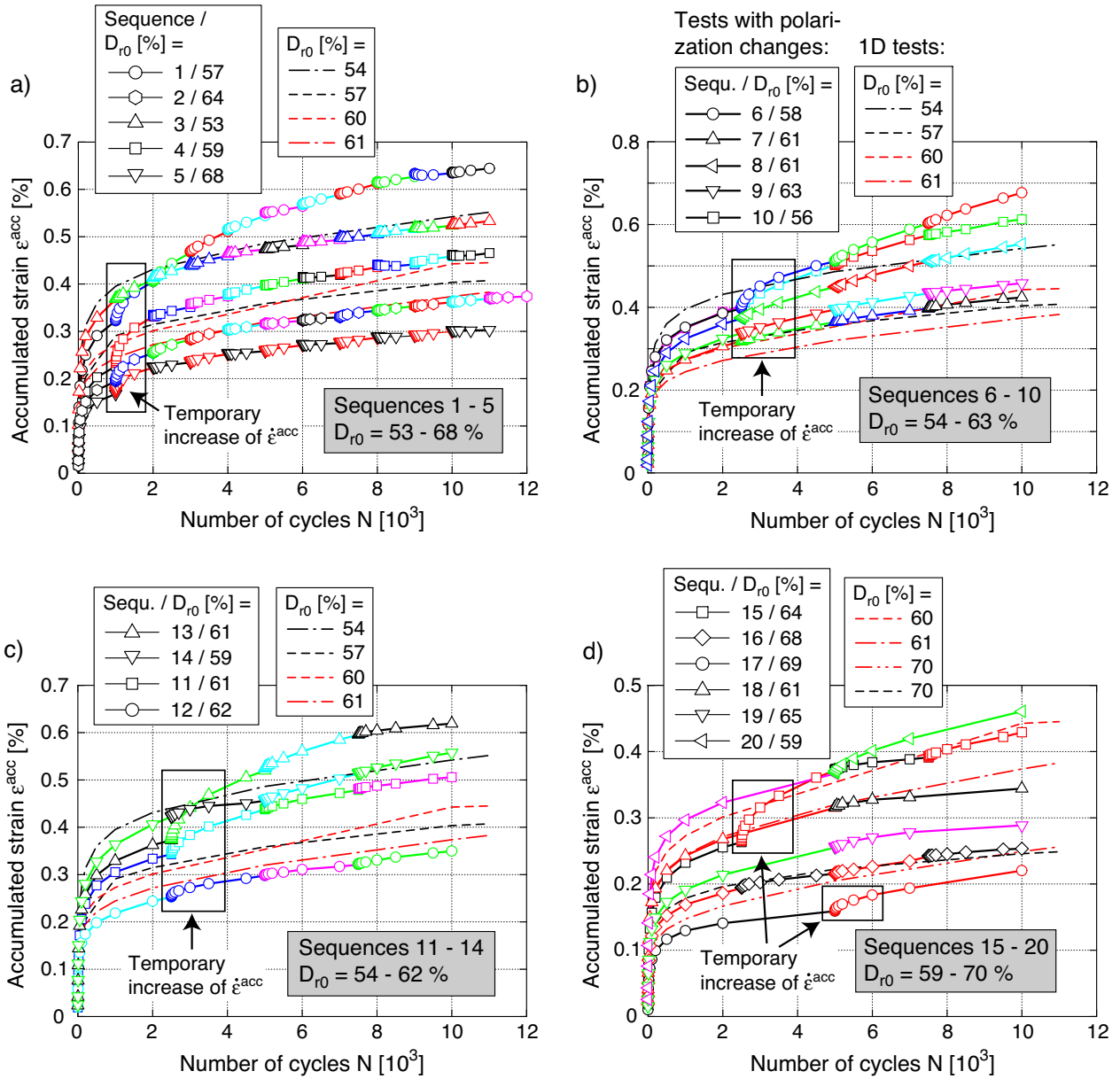


Fig. 9: Development of accumulated strain $\epsilon^{acc}(N)$ measured for medium dense specimens ($53\% \leq D_{r0} \leq 70\%$) in drained cyclic triaxial tests with packages of cycles applied with different polarizations and in various sequences. The polarizations are distinguished by choosing the same colours as used in Figures 6 and 7. The results from the reference tests without polarization change (1D tests) are given as the dashed curves.

or 2 to 5 corresponds to an angle $\Delta\alpha_{PQ} = 90^\circ$, while a variation from 4 to 1 or 5 to 2 leads to $\Delta\alpha_{PQ} = -90^\circ$. The three diagrams in Figure 11 contain the data for the three different density ranges. The sequence of the polarizations is indicated by the description $i \rightarrow j$, with i and j being the polarizations before and after the change. Evidently, despite the considerable scatter of the data in Figure 11, the increase of the accumulation rate due to the polarization change is maximal for $\Delta\alpha_{PQ} = 90^\circ$ (e.g. 1 \rightarrow 4), but not for -90° (e.g. 4 \rightarrow 1). The smallest effect of the first polarization change is observed at $\Delta\alpha_{PQ} \approx -30^\circ$. No clear correlation with the number of previously applied cycles or with soil density can be concluded from Figure 11.

Figure 12a presents the residual strain after 10,000 cycles in dependence of initial relative density. The different symbols distinguish between different numbers of polarization

changes during the cyclic loading. The data do hardly show any clear differences between the tests with 9 polarization changes and those with constant polarization. The same applies to the tests with a single change. Surprisingly, the effect is more pronounced in case of the tests with three such alterations of polarization. Almost independent of initial density, the tests with three polarization changes delivered an about $\Delta\epsilon^{acc} = 0.1$ to 0.2% larger residual strain than those with a lower or higher number of α_{PQ} alterations.

The $\epsilon_q^{acc} - \epsilon_v^{acc}$ data at $N = 10,000$ shown in Figure 12b do not show any noticeable effect of the number of polarization changes conducted during these cycles. Also the $\epsilon_q^{acc} - \epsilon_v^{acc}$ strain paths measured in the individual tests confirm that the direction of strain accumulation is not altered by the multiple changes of the direction of the cycles.

Based on Figures 9, 10 and 12 it can be concluded that

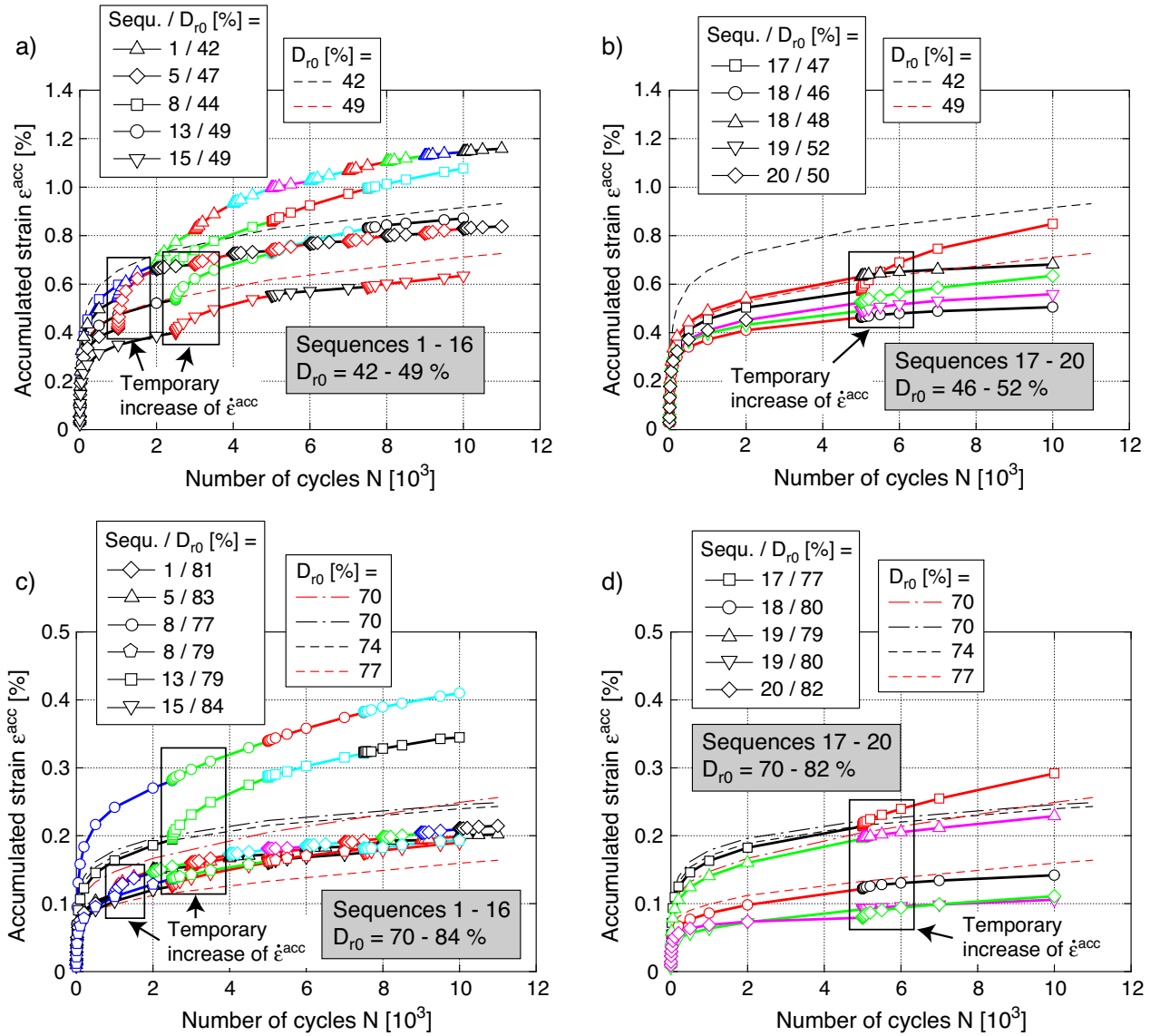


Fig. 10: Development of accumulated strain $\epsilon^{acc}(N)$ measured for lower ($42\% \leq D_{r0} \leq 52\%$) or higher densities ($70\% \leq D_{r0} \leq 84\%$) in drained cyclic triaxial tests with packages of cycles applied with different polarizations and in various sequences. The polarizations are distinguished by choosing the same colours as used in Figures 6 and 7. The results from the reference tests without polarization change (1D tests) are given as the dashed curves.

the influence of multiple polarization changes on the final residual strain may be regarded as less important than previously thought, based on the experiments presented in [22] (Figure 1) or [5]. It seems relevant for the first change of the polarization only and has only a moderate effect on the residual strain after a larger number of cycles. Thus the factor f_π of the HCA model, describing the effect of polarization changes, could possibly be omitted. A moderate increase of the rate of strain accumulation (e.g. via a 20% increase of parameter C_{N1} , see Appendix) for problems with multiple polarization changes could be sufficient for practical purposes.

It should be kept in mind, however, that although the effect of polarization changes may be of minor importance on the element test level, it can be of relevance for foundation systems. For example, in case of piles (e.g. [3, 13, 14]) the change of the cyclic loading direction goes along with a change of the region of soil involved in strain accumulation or stress relaxation. Zones with low cumulative effects

before the polarization change may be subjected to a large cyclic impact afterwards, and vice versa. Such influence of polarization changes on the foundation level can be studied in FE simulations with the HCA model. However, such simulations are beyond the scope of the present paper.

5 Summary, conclusions and outlook

About 50 drained cyclic triaxial tests with a simultaneous harmonic oscillation of the axial and the horizontal effective stress have been performed in order to study the influence of sudden polarization changes, i.e. alterations of the direction of the cyclic loading. Six different polarizations were tested in different sequences. The difference in angle $\Delta\alpha_{PQ}$ between adjacent polarizations was 30 degrees in the isometric P - Q plane. The polarization was changed every 1000, 2500 or 5000 cycles. In total at least 10,000 cycles were applied to each specimen. For comparison purpose several reference tests with a constant polarization

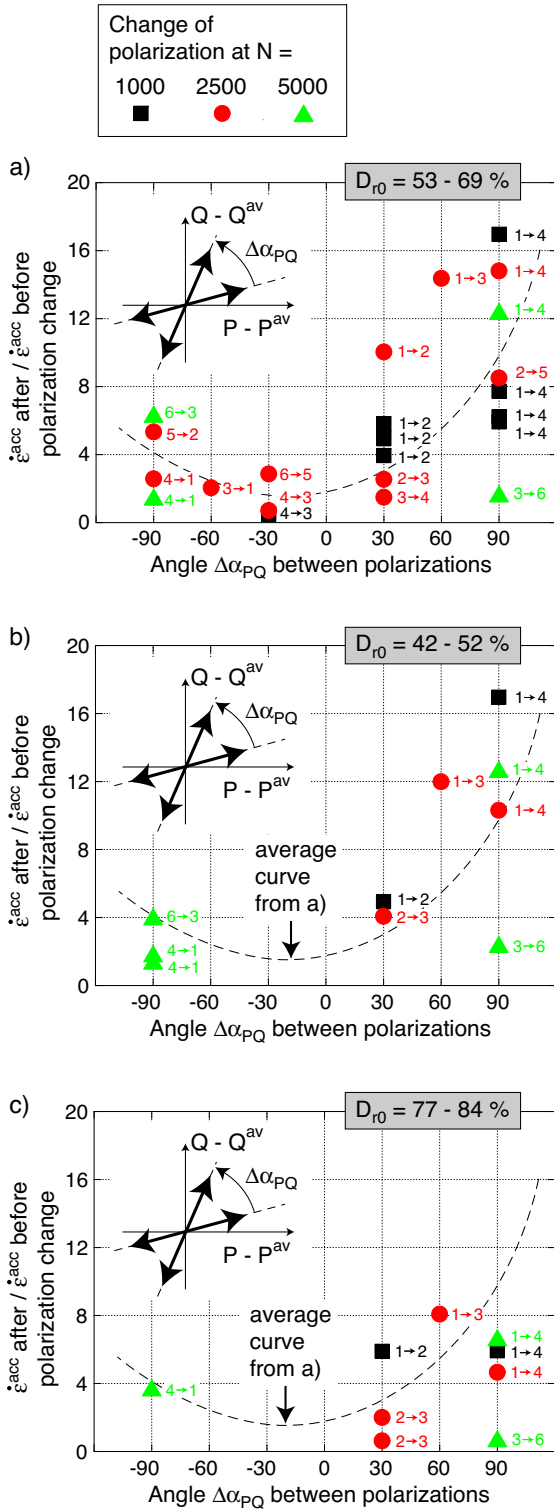


Fig. 11: Ratio of the rates of strain accumulation $\dot{\epsilon}^{\text{acc}}$ directly before and directly after the first polarization change as a function of the angle $\Delta\alpha_{PQ}$ between both polarizations. The sequence of the polarizations is indicated by $i \rightarrow j$.

throughout the whole test were also performed. The initial density was varied between loose and dense.

Based on the data from the first 1000 cycles (before the first polarization change) it can be concluded that the rate of strain accumulation is independent of the polarization itself. This enables the analysis of the effect of polarization changes. The tests revealed that the first polarization change leads to a temporary increase of the rate of strain accumulation, while all further alterations have only a marginal effect on the strain accumulation curves $\dot{\epsilon}^{\text{acc}}(N)$. The effect of the first polarization change, quantified by the quotient of the strain accumulation rates directly after and before the change, is stronger for larger angles $\Delta\alpha_{PQ}$ between both polarizations. A change from a purely deviatoric to a purely isotropic polarization has a larger effect than an alteration in the opposite direction. No clear correlation between the temporary increase of the strain accumulation rate with the number of cycles applied prior to the polarization change or density can be derived from the collected data. Considering a constant density, the tests with 1 and 9 polarization changes delivered almost the same residual strain after 10,000 cycles as the reference tests without any polarization change. In contrast, 3 polarization changes during the 10,000 applied cycles lead to 10 to 20 % higher final accumulated strains. The direction of deviatoric and volumetric strain accumulation rates, was found unaffected by the multiple polarization changes.

Based on the present study it can be concluded that the effect of multiple polarization changes on the cumulative deformations after a large number of cycles is less significant than expected from earlier simple shear test studies. For a practical application of the high-cycle accumulation model of Niemunis et al. [11] to problems with multiple polarization changes the factor f_{π} describing the effect of polarization changes may be omitted. It seems sufficient to increase the overall intensity of accumulation, described by the function f_N and its parameter C_{N1} , by 10 to 20 % to capture the effect of repeated alterations of the cyclic loading direction.

In future it is intended to study the effect of polarization changes for specimens with a different initial fabric (preparation by moist tamping). Furthermore, it will be investigated if a continuous change of the direction of cyclic loading (i.e. a small $\Delta\alpha_{PQ}$ applied after each cycle) leads to larger cumulative rates. An analysis on the micromechanical level will provide a better understanding of the experimental observations. Finally, it should be stressed that although polarization changes seem to be of minor importance on the element test level they can have larger effects in case of foundation systems.

Acknowledgements

The presented study has been funded by the Federal Ministry for the Environment, Nature Conservation and Nuclear Safety (BMU) as part of the project "Geotechnical robustness and self-healing of foundations for offshore wind power plants" (grant No. 0327618). The authors are grateful to BMU for the financial support. The cyclic tests have been performed by the technician H. Borowski in the IBF soil mechanics laboratory.

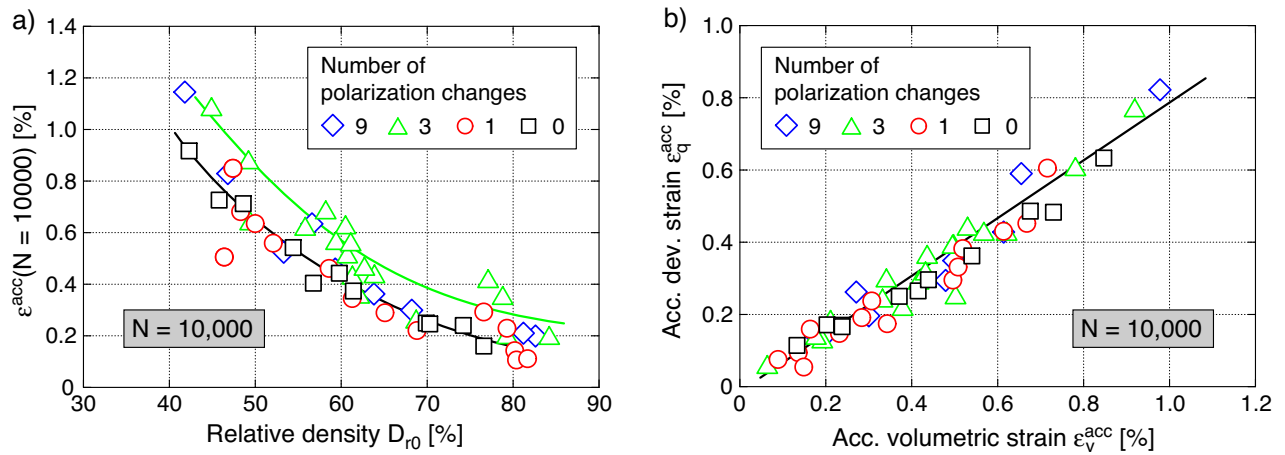


Fig. 12: a) Accumulated strain ϵ_q^{acc} after 10,000 cycles as a function of initial relative density D_{r0} , b) Accumulated deviatoric strain ϵ_q^{acc} as a function of accumulated volumetric strain ϵ_v^{acc} after 10,000 cycles

References

- [1] M. Budhu. Nonuniformities imposed by simple shear apparatus. *Canadian Geotechnical Journal*, 21(1):125–137, 1984.
- [2] V.A. Dyaljee and G.P. Raymond. Repetitive load deformation of cohesionless soil. *Journal of the Geotechnical Engineering Division, ASCE*, 108(GT10):1215–1229, 1982.
- [3] J. Dührkop and J. Grabe. Monopilegründungen von Offshore-Windenergieanlagen - zum Einfluss einer veränderlichen zyklischen Lastangriffsrichtung. *Bautechnik*, 85(5):317–321, 2008.
- [4] P.M. Duku, J.P. Stewart, D.H. Whang, and E. Yee. Volumetric strains of clean sands subject to cyclic loads. *Journal of Geotechnical and Geoenvironmental Engineering, ASCE*, 134(8):1073–1085, 2008.
- [5] V. H. Le. Zum Verhalten vom Sand unter zyklischer Beanspruchung mit Polarisationswechsel im Einfachscherversuch. Dissertation, Fachgebiet Grundbau und Bodenmechanik, Technische Universität Berlin, Issue No. 66, 2015.
- [6] C. Leblanc, G.T. Hously, and B.W. Byrne. Response of stiff piles in sand to long-term cyclic lateral loading. *Géotechnique*, 60(2):79–90, 2010.
- [7] J.H. Long and G. Vanneste. Effects of cyclic lateral loads on piles in sand. *Journal of Geotechnical Engineering, ASCE*, 120(1):225–244, 1994.
- [8] S. López-Querol and M.R. Coop. Drained cyclic behaviour of loose Dogs Bay sand. *Géotechnique*, 62(4):281–289, 2012.
- [9] H. Matsuoka and T. Nakai. A new failure criterion for soils in three-dimensional stresses. In *Deformation and Failure of Granular Materials*, pages 253–263, 1982. Proc. IUTAM Symp. in Delft.
- [10] A. Niemunis. Extended hypoplastic models for soils. Habilitation, Veröffentlichungen des Institutes für Grundbau und Bodenmechanik, Ruhr-Universität Bochum, Heft Nr. 34, 2003. available from www.pg.gda.pl/~aniem/an-liter.html.
- [11] A. Niemunis, T. Wichtmann, and Th. Triantafyllidis. A high-cycle accumulation model for sand. *Computers and Geotechnics*, 32(4):245–263, 2005.
- [12] F. Rosquoet, L. Thorel, J. Garnier, and Y. Canepa. Lateral cyclic loading of sand-installed piles. *Soils and Foundations*, 47(5):821–832, 2007.
- [13] C. Rudolph, B. Bienen, and J. Grabe. Effect of variation of the loading direction on the displacement accumulation of large-diameter piles under cyclic lateral loading in sand. *Canadian Geotechnical Journal*, 51(10):1196–1206, 2014.
- [14] C. Rudolph and J. Grabe. Untersuchungen zu zyklisch horizontal belasteten Pfählen bei veränderlicher Lastrichtung. *Bautechnik*, 36(2):90–95, 2013.
- [15] M.L. Silver and H.B. Seed. Volume changes in sands during cyclic loading. *Journal of the Soil Mechanics and Foundations Division, ASCE*, 97(SM9):1171–1182, 1971.
- [16] A.S.J. Suiker, E.T. Selig, and R. Frenkel. Static and cyclic triaxial testing of ballast and subballast. *Journal of Geotechnical and Geoenvironmental Engineering, ASCE*, 131(6):771–782, 2005.
- [17] H.E. Taşan, F. Rackwitz, and S. Savidis. Experimentelle Untersuchungen zum Verhalten von zyklisch horizontal belasteten Monopiles. *Bautechnik*, 88(2):102–112, 2011.
- [18] T. Tokue. Deformation behaviours of dry sand under cyclic loading and a stress-dilatancy model. *Soils and Foundations*, 19(2):63–78, 1979.
- [19] T. Wichtmann. Explicit accumulation model for non-cohesive soils under cyclic loading. PhD thesis, Publications of the Institute of Soil Mechanics and Foundation Engineering, Ruhr-University Bochum, Issue No. 38, 2005.
- [20] T. Wichtmann. Soil behaviour under cyclic loading - experimental observations, constitutive description and applications. Habilitation thesis, Publications of the Institute of Soil Mechanics and Rock Mechanics, Karlsruhe Institute of Technology, Issue No. 181, 2016.
- [21] T. Wichtmann, A. Niemunis, and Th. Triantafyllidis. Strain accumulation in sand due to cyclic loading; drained triaxial tests. *Soil Dynamics and Earthquake Engineering*, 25(12):967–979, 2005.
- [22] T. Wichtmann, A. Niemunis, and Th. Triantafyllidis. On the influence of the polarization and the shape of the strain loop on strain accumulation in sand under high-cyclic loading. *Soil Dynamics and Earthquake Engineering*, 27(1):14–28, 2007.
- [23] T. Wichtmann, A. Niemunis, and Th. Triantafyllidis. Improved simplified calibration procedure for a high-cycle accumulation model. *Soil Dynamics and Earthquake Engineering*, 70(3):118–132, 2015.
- [24] T. Wichtmann and Th. Triantafyllidis. Strain accumulation due to packages of cycles with varying amplitude and/or

average stress - on the bundling of cycles and the loss of the cyclic preloading memory. *Soil Dynamics and Earthquake Engineering*, 101:250–263, 2017.

- [25] Y. Yamada and K. Ishihara. Yielding of loose sand in three-dimensional stress conditions. *Soils and Foundations*, 22(3):15–31, 1982.
- [26] E. Yee, P. M. Duku, and J. P. Stewart. Cyclic volumetric strain behavior of sands with fines of low plasticity. *Journal of Geotechnical and Geoenvironmental Engineering, ASCE*, 140:1–10, 2014.

Appendix: Equations of the HCA model

The HCA model has been originally proposed by Niemunis et al. [11] in 2005. The model is based on the comprehensive experimental parametric study documented in [19, 21, 22]. The basic equation of the HCA model reads

$$\dot{\boldsymbol{\sigma}} = \mathbf{E} : (\dot{\boldsymbol{\varepsilon}} - \dot{\boldsymbol{\varepsilon}}^{\text{acc}} - \dot{\boldsymbol{\varepsilon}}^{\text{pl}}) \quad (5)$$

with the stress rate $\dot{\boldsymbol{\sigma}}$ of the effective Cauchy stress $\boldsymbol{\sigma}$ (compression positive), the strain rate $\dot{\boldsymbol{\varepsilon}}$ (compression positive), the strain accumulation rate $\dot{\boldsymbol{\varepsilon}}^{\text{acc}}$, a plastic strain rate $\dot{\boldsymbol{\varepsilon}}^{\text{pl}}$ (necessary only for stress paths touching the yield surface) and the barotropic elastic stiffness \mathbf{E} . In the context of HCA models the dot over a symbol means a derivative with respect to the number of cycles N (instead of time t), i.e. $\dot{\square} = \partial \square / \partial N$. Depending on the boundary conditions, Eq. (5) predicts either a change of average stress ($\dot{\boldsymbol{\sigma}} \neq \mathbf{0}$) or an accumulation of residual strain ($\dot{\boldsymbol{\varepsilon}} \neq \mathbf{0}$) or both.

For the strain accumulation rate $\dot{\boldsymbol{\varepsilon}}^{\text{acc}}$ in Eq. (5) the following multiplicative approach is used:

$$\dot{\boldsymbol{\varepsilon}}^{\text{acc}} = \dot{\boldsymbol{\varepsilon}}^{\text{acc}} \mathbf{m} \quad (6)$$

with the *direction* of strain accumulation (flow rule) $\mathbf{m} = \dot{\boldsymbol{\varepsilon}}^{\text{acc}} / \|\dot{\boldsymbol{\varepsilon}}^{\text{acc}}\| = (\dot{\boldsymbol{\varepsilon}}^{\text{acc}})^{\rightarrow}$ (unit tensor) and the *intensity* of strain accumulation $\dot{\boldsymbol{\varepsilon}}^{\text{acc}} = \|\dot{\boldsymbol{\varepsilon}}^{\text{acc}}\|$. The flow rule of the modified Cam clay (MCC) model has been found suitable for \mathbf{m} :

$$\mathbf{m} = \left[\frac{1}{3} \left(p^{\text{av}} - \frac{(q^{\text{av}})^2}{M^2 p^{\text{av}}} \right) \mathbf{1} + \frac{3}{M^2} (\boldsymbol{\sigma}^{\text{av}})^* \right]^{\rightarrow} \quad (7)$$

where $\square^{\rightarrow} = \square / \|\square\|$ denotes the normalization of a tensorial quantity, while \square^* is the deviatoric part of \square . For the triaxial case the critical stress ratio $M = F M_{cc}$ is calculated with

$$F = \begin{cases} 1 + M_{cc}/3 & \text{for } \eta^{\text{av}} \leq M_{cc} \\ 1 + \eta^{\text{av}}/3 & \text{for } M_{cc} < \eta^{\text{av}} < 0 \\ 1 & \text{for } \eta^{\text{av}} \geq 0 \end{cases} \quad (8)$$

wherein

$$M_{cc} = \frac{6 \sin \varphi_{cc}}{3 - \sin \varphi_{cc}} \quad \text{and} \quad M_{ec} = -\frac{6 \sin \varphi_{cc}}{3 + \sin \varphi_{cc}} \quad (9)$$

with a parameter φ_{cc} .

The intensity of strain accumulation $\dot{\boldsymbol{\varepsilon}}^{\text{acc}}$ in Eq. (6) is calculated as a product of six functions:

$$\dot{\boldsymbol{\varepsilon}}^{\text{acc}} = f_{\text{ampl}} \dot{f}_N f_e f_p f_Y f_{\pi} \quad (10)$$

each considering a single influencing parameter (see Table 3), i.e. the strain amplitude $\varepsilon^{\text{ampl}}$ (function f_{ampl}), the cyclic preloading g^A (\dot{f}_N), void ratio e (f_e), average mean

Function	Material constants
$f_{\text{ampl}} = \min \left\{ \left(\frac{\varepsilon^{\text{ampl}}}{10^{-4}} \right)^{C_{\text{ampl}}}; 10^{C_{\text{ampl}}} \right\}$	C_{ampl}
$\dot{f}_N = \dot{f}_N^A + \dot{f}_N^B$	C_{N1}
$\dot{f}_N^A = C_{N1} C_{N2} \exp \left[-\frac{g^A}{C_{N1} f_{\text{ampl}}} \right]$	C_{N2}
$\dot{f}_N^B = C_{N1} C_{N3}$	C_{N3}
$f_e = \frac{(C_e - e)^2}{1 + e} \frac{1 + e_{\text{max}}}{(C_e - e_{\text{max}})^2}$	C_e
$f_p = \exp \left[-C_p \left(\frac{p^{\text{av}}}{100 \text{ kPa}} - 1 \right) \right]$	C_p
$f_Y = \exp(C_Y \bar{Y}^{\text{av}})$	C_Y
$f_{\pi} = 1 + C_{\pi 1} (1 - \cos \alpha)$	$C_{\pi 1}$
$\dot{\alpha} = -C_{\pi 2} \alpha (\varepsilon^{\text{ampl}})^2$	$C_{\pi 2}$

Table 3: Summary of the functions and material constants of the HCA model

pressure p^{av} (f_p), average stress ratio η^{av} or \bar{Y}^{av} (f_Y) and the effect of polarization changes (f_{π}).

The normalized stress ratio \bar{Y}^{av} used in f_Y is zero for isotropic stresses ($\eta^{\text{av}} = 0$) and one on the critical state line ($\eta^{\text{av}} = M_{cc}$). The function Y of Matsuoka & Nakai [9] is used for that purpose:

$$\bar{Y}^{\text{av}} = \frac{Y^{\text{av}} - 9}{Y_c - 9} \quad \text{with} \quad Y_c = \frac{9 - \sin^2 \varphi_{cc}}{1 - \sin^2 \varphi_{cc}} \quad (11)$$

$$Y^{\text{av}} = \frac{27(3 + \eta^{\text{av}})}{(3 + 2\eta^{\text{av}})(3 - \eta^{\text{av}})} \quad (12)$$

For a constant strain amplitude, the function f_N simplifies to:

$$f_N = C_{N1} [\ln(1 + C_{N2} N) + C_{N3} N] \quad (13)$$

The HCA model incorporates a tensorial definition of the strain amplitude. The norm $\varepsilon^{\text{ampl}} = \|\mathbf{A}_{\varepsilon}\|$ of the tensorial strain amplitude \mathbf{A}_{ε} (fourth-order tensor) enters the amplitude function f_{ampl} . The normalized amplitude $\vec{\mathbf{A}}_{\varepsilon} = \mathbf{A}_{\varepsilon} / \|\mathbf{A}_{\varepsilon}\|$ (also a fourth-order tensor) is termed polarization. Another fourth-order tensor $\boldsymbol{\pi}$ called back polarization is used for a weighted memorizing of the polarization of the cycles in the past. The angle between the actual polarization $\vec{\mathbf{A}}_{\varepsilon}$ and the back polarization $\boldsymbol{\pi}$ is termed α ($\alpha = \arccos(\vec{\mathbf{A}}_{\varepsilon} :: \boldsymbol{\pi})$ with $::$ denoting a quadruple contraction of two fourth order tensors, resulting in a scalar variable) and enters the function f_{π} :

$$f_{\pi} = 1 + C_{\pi 1} (1 - \cos \alpha) \quad (14)$$

with a material constant $C_{\pi 1}$. If a package of cycles is directly followed by another package with the same polarization, i.e. $\alpha = 0$, then no correction of the accumulation rate is needed and $f_{\pi} = 1$. If the polarization changes by an angle α then the rate of strain accumulation is immediately increased by the factor f_{π} . The material constant $C_{\pi 1}$ can thus be calibrated based on the jump in the strain accumulation rate caused by a polarization change. During cycles with $\vec{\mathbf{A}}_{\varepsilon} = \text{constant}$ the tensor $\boldsymbol{\pi}$ is evolving (rotating) towards the current polarization, $\boldsymbol{\pi} \rightarrow \vec{\mathbf{A}}_{\varepsilon}$. The evolution of

the angle α is described by

$$\dot{\alpha} = -C_{\pi_2} \alpha (\varepsilon^{\text{ampl}})^2 \quad (15)$$

with another material constant C_{π_2} . In order to rotate the tensor $\boldsymbol{\pi}$ by the angle $\Delta\alpha = \dot{\alpha}\Delta N$ an eighth-order tensor \mathbf{R} is used [11].